Available online at www.sciencedirect.com
SCIENCE DIRECT®
Journal of Sound and Vibration 291 (2006) 285–301
JOURNAL OF SOUND AND VIBRATION
www.elsevier.com/locate/jsvi

Wavelet transform-based modal parameter identification considering uncertainty

B.F. Yan[a], A. Miyamoto[a,*], E. Brühwiler[b]

[a]*Department of Computer & Systems Engineering, Yamaguchi University, 2-16-1 Tokiwadai, Ube, 755-8611 Yamaguchi, Japan*
[b]*Institute of Maintenance and Safety of Structures (MCS-ENAC), Swiss Federal Institute of Technology (EPFL), CH-1015 Lausanne EPFL, Switzerland*

Received 3 August 2004; received in revised form 19 April 2005; accepted 9 June 2005
Available online 2 September 2005

Abstract

This paper presents an integrated identification method to consider the uncertainty effect on modal parameters for output-only system. The method is based on the time–frequency characteristics of the wavelet transform (WT) and the capabilities of the bootstrap distribution in statistical estimation. For the WT-only based identification method, the important issues related to identification accuracy such as modal separation, end-effect, associated with the parameter selection of wavelet function based on Shannon entropy, are given detailed investigations. The bootstrap procedure is then employed to evaluate the uncertainty effects by providing confidence interval of the modal parameter statistically. The effectiveness of the integrated method has been confirmed through numerical simulation and experimental test on a bridge model.

1. Introduction

There are numerous approaches that can be applied to extract modal parameters of structure [1,2]. Traditionally, modal parameters are extracted by performing the reducing and curve-fitting

*Corresponding author. Tel./fax: +81 836 85 9530.
E-mail addresses: yanbanfu@design.csse.yamaguchi-u.ac.jp (B.F. Yan), miyamoto@design.csse.yamaguchi-u.ac.jp (A. Miyamoto), eugen.bruehwiler@epfl.ch (E. Brühwiler).

0022-460X/$ - see front matter © 2005 Elsevier Ltd. All rights reserved.
doi:10.1016/j.jsv.2005.06.005

procedures either on series of measured frequency response function or on time response, such as impulse response function and free-decay response. The frequency domain approaches based on the discrete Fourier transform (DFT) have some drawbacks such as leakage, aliasing, requiring large amounts of data or test for averaging, and rich frequency spectrum for the input signals [3]. Moreover, the DFT is commonly accurate for calculating the frequency content of a stationary signal. Therefore when applied to a non-stationary signal, the DFT provides signal's average characteristics over the time-period, and smears its local behavior globally. Although the modified version of the Fourier transform termed short-time Fourier transform (STFT) can resolve some of the problems associated with non-stationary signals, it does not address all issues of concern [4,5].

For large-scale civil engineering structures such as bridges, towers, offshore platforms, etc. in operating conditions, it is not suitable to excite the structure using artificial inputs and to measure actual excitation, accordingly. Recently, the time-domain-based identification schemes particularly in the case where no input but only response measurements are available have received considerable attentions. The output-only based techniques include autoregressive moving average vector (ARMAV) model [6], stochastic subspace identification (SSI) method [7], and the eigensystem realization algorithm (ERA) [8,9]. One disadvantage of these approaches is that they use a large number of important matrices, which require time-consuming computation. In addition, the noise levels of the response data also have significant effects on the identification accuracies.

In order to overcome the weakness of the Fourier-based approach in providing indirect or incomplete information on capturing time-varying features of structure, some new tools such as Wigner–Ville distribution, wavelet transform (WT) and Hilbert–Huang transform (HHT) capable of yielding a time–frequency representation are developed to construct new frameworks for system identification and damage detection [5,10–14]. The WT has the ability to decouple the measured multicomponent signal to monocomponent signals in the form of complex-valued signature via the popular Morlet wavelet, and then the identification scheme for single-degree-of-freedom (sdof) system can be implemented to extract the modal parameters. It is important to note that the time and frequency resolutions of the WT have significant impacts on the identification accuracy, which needs to be clarified by theoretical analysis.

For the structure subjected to the ambient loading, the WT method is generally applied in conjunction with the well-known random decrement technique (RDT) to identify the modal parameters [12,13]. Note that the WT as well as the traditional schemes can only supply a single estimate of the modal parameter for each time history, and the repeated measurements for the real structure are also restricted. Moreover, due to the impacts of unmeasurable ambient excitation sources, noise contamination, environmental variability, and measurement error, the ambient excitation acted upon the real structure, in a strict sense, generally does not apply for the RDT's assumption that the unknown excitation forces are Gaussian white noise. Subsequently, the uncertainty, to a certain extent, will cause possible estimation errors no matter what kind of identification methods are adopted. Practically, due to the nature of the ambient excitation, a statistical description of the identification procedure is appropriate to consider and assess the uncertainty.

To make up for the inadequacy of the WT-only based modal identification, a statistical tool termed bootstrap [15] is proposed to evaluate the effects of uncertainty according to the statistical characteristics of the modal parameters. This paper is organized into 5 sections. Section 1 is

introduction. In Section 2, a WT-only based modal identification method adopting modified Morlet wavelet is performed with the special emphases on the time–frequency resolution and optimal parameter selection of wavelet function. Section 3 proposes a bootstrap scheme to consider the uncertainty effect. In Section 4, the integrated method is verified through numerical simulation on a damped system with closely spaced modes and an experimental test on a bridge model. Finally, the conclusions are presented in Section 5.

2. Wavelet transform-based modal identification

2.1. Modified complex morlet wavelet

The WT is a linear representation, which sums all time of the signal $x(t)$ multiplied by scaled, shifted versions of the mother wavelet $\psi(t)$ in the form

$$W(a,b)=\frac{1}{\sqrt{a}}\int_{-\infty}^{+\infty}x(t)\psi^{*}\left(\frac{t-b}{a}\right)\mathrm{d}t, \tag{1}$$

where "*" denotes the complex conjugation. The scale index a controls the stretch of the analysis window and parameter b indicates the time shifting. The factor $1/\sqrt{a}$ is used to ensure energy preservation. The wavelet coefficient $W(a,b)$ measures the similarity between the signal $x(t)$ and each wavelet function in the form of time–frequency representation. Hence, the dominant frequency components of the signal create wavelet coefficients with prominent amplitudes and this is the basis of the WT-based modal identification.

There are different types of real- and complex-valued wavelet functions for various purposes. One of the most popular and widely used is the complex Morlet wavelet due to its capabilities in time–frequency localization for analytical signal. In this study, the modified complex Morlet wavelet function is used and formulated as

$$\psi(t)=\frac{1}{\sqrt{\pi f_b}}\left(\mathrm{e}^{\mathrm{j}2\pi f_c t}-\mathrm{e}^{-f_b(\pi f_c)^2}\right)\mathrm{e}^{-t^2/f_b}, \tag{2}$$

where f_b is the bandwidth parameter, f_c is the central wavelet frequency, and j is the imaginary unit. The dilated version of the Fourier transform of $\psi(t)$ is given by

$$\Psi(af)=\mathrm{e}^{-\pi^2 f_b(af-f_c)^2}-\mathrm{e}^{-\pi^2 f_b((af)^2+f_c^2)}. \tag{3}$$

Note that let $f=0$, the frequency response $\Psi(af)=0$, which implies that the integral of the mother wavelet $\psi(t)$ over the entire time domain is zero. Hence, the mother wavelet function satisfies the admissibility condition. Practically, when we assume $\sqrt{f_b}f_c\geqslant\sqrt{2}$, the term $\mathrm{e}^{-f_b(\pi f_c)^2}$ in Eq. (2) can be viewed as a negligible quantity [17], thus the approximate version of the modified Morlet wavelet and its dilated Fourier transform are, respectively, expressed as

$$\psi(t)=\frac{1}{\sqrt{\pi f_b}}\mathrm{e}^{\mathrm{j}2\pi f_c t}\mathrm{e}^{-t^2/f_b}, \tag{4}$$

$$\Psi(af)=\mathrm{e}^{-\pi^2 f_b(af-f_c)^2}. \tag{5}$$

Note that $\Psi(af)$ reaches the maximum value when $af = f_c$, which demonstrates that the localized Fourier frequency f is determined by the parameters a and f_c.

2.2. Modal parameter determination

Consider a linear damped multi-degree-of-freedom (mdof) system with n real modes, its free decay response is given as

$$x(t) = \sum_{i=1}^{n} A_i e^{-2\pi\zeta_i f_i t} \cos(2\pi f_{di} t + \theta_i), \tag{6}$$

where A_i is the amplitude of the ith mode, θ_i is the phase angle, f_i is the ith undamped natural frequency, $f_{di} = f_i\sqrt{1-\zeta_i^2}$ is the damped natural frequency, and ζ_i is the damping ratio.

By substituting Eqs. (4) and (6) into Eq. (1), the Morlet wavelet coefficients of the free decay signal can be approximated by means of asymptotic techniques [10,11] as follows:

$$W(a,b) = \frac{\sqrt{a}}{2}\sum_{i=1}^{n} A_i e^{-2\pi\zeta_i f_i b} e^{-\pi^2 f_b (af_i - f_c)^2} e^{j(2\pi f_{di} b + \theta_i)}. \tag{7}$$

By localizing a fixed value of the scale parameter $a = a_i$, the term $e^{-\pi^2 f_b (af_i - f_c)^2}$ obtains its maximum value at $a_i = f_c/f_i$. In such cases, only the mode i related to the scale a_i gives a significant contribution to Eq. (7), while the other $(n-1)$ modes appear to be negligible. Note that the quality of above approximation is dependent on the coupling effects between modes. For the system with not strong closely spaced modes, the wavelet coefficient at scale a_i can be written in the form

$$W(a_i,b) = \frac{\sqrt{a_i}}{2} A_i e^{-2\pi\zeta_i f_i b} e^{j(2\pi f_{di} b + \theta_i)}, \tag{8}$$

which implies that the WT is capable of decomposing a multicomponent signal to single modes and representing them in the form of complex-valued signals. Next by substituting t for b, Eq. (8) can be rewritten in the form of time-varying amplitude $B_i(t)$ and phase angle $\varphi_i(t)$.

$$W(a_i,t) = \frac{\sqrt{a_i}}{2} A_i e^{-2\pi\zeta_i f_i t} e^{j(2\pi f_{di} t + \theta_i)} = B_i(t) e^{j\varphi_i(t)} \tag{9}$$

and applying logarithmic and derivative operators to $B_i(t)$ and $\varphi_i(t)$, respectively, we obtain

$$\ln B_i(t) = -2\pi\zeta_i f_i t + \ln\left(\frac{\sqrt{a_i}}{2} A_i\right) \Rightarrow \frac{\mathrm{d}\ln B_i(t)}{\mathrm{d}t} = -2\pi\zeta_i f_i, \tag{10}$$

$$\frac{\mathrm{d}\varphi_i(t)}{\mathrm{d}t} = 2\pi f_{di} = 2\pi f_i\sqrt{1-\zeta_i^2}. \tag{11}$$

Consequently, the slopes of $\ln B_i(t)$ and $\varphi_i(t)$ can be combined to identify the natural frequency f_i and the damping ratio ζ_i as follows:

$$f_i = \sqrt{\left(\frac{\mathrm{d}\ln B_i(t)}{\mathrm{d}t}\right)^2 + \left(\frac{\mathrm{d}\varphi_i(t)}{\mathrm{d}t}\right)^2} \Big/ 2\pi, \tag{12}$$

$$\zeta_i = -\left(\frac{\mathrm{d}\ \ln\ B_i(t)}{\mathrm{d}t}\right) \Big/ 2\pi f_i. \tag{13}$$

In general, the linear least-squares fitting technique is applied to the wavelet phases and amplitude curves for effective determination.

2.3. Resolution property

Because of the nature of the WT, the resolution properties having inevitable influences on the identification accuracies of the modal parameters should be taken into account. A research conducted by Kijewski and Kareem [12] investigated the impacts of modal separation and end-effect on the time–frequency resolution and suggested guidelines for parameter selection. This study extends their method from traditional Morlet wavelet to modified Morlet wavelet, and particularly uses the Shannon wavelet entropy to select the optimum critical parameters.

2.3.1. Time–frequency resolution

When discussing the joint time–frequency resolution, the Heisenberg uncertainty principle provides a good performance indicator termed time–frequency resolution rectangle $\Delta t \Delta f \geqslant \frac{1}{4}\pi$ to evaluate the time–frequency representation [4]. For the modified Morlet wavelet adopting a Gaussian function as described in Eq. (4), the resolution rectangle holds equality, i.e. $\Delta t_\psi \Delta f_\psi = \frac{1}{4}\pi$. Moreover, the frequency-domain standard deviation can be employed to measure a signal's frequency bandwidth by using characterization of time waveform and power spectrum [4]. Considering the resolution rectangle, the time and frequency resolutions of the modified Morlet wavelet can be written as

$$\Delta t_\psi = \frac{\sqrt{f_b}}{2}, \qquad \Delta f_\psi = \frac{1}{2\pi\sqrt{f_b}}. \tag{14}$$

Note that the time and frequency resolutions of the WT are dependent on the mother wavelet function [10]. Considering $a_i = f_c/f_i$ and Eq. (14), one obtains

$$\Delta t_i = a_i \Delta t_\psi = \frac{f_c}{f_i}\frac{\sqrt{f_b}}{2}, \qquad \Delta f_i = \frac{1}{a_i}\Delta f_\psi = \frac{f_i}{f_c}\frac{1}{2\pi\sqrt{f_b}}, \tag{15}$$

which indicates that the parameters f_b and f_c can be adjusted to obtain appropriate time and frequency resolutions.

More generally, from the viewpoint of modal separation, in order to separate two closely spaced frequency components f_i and f_{i+1} with a difference of $\Delta f_{i,i+1} = f_{i+1} - f_i$ and an average of $f_{i,i+1} = (f_i + f_{i+1})/2$, by substituting $\Delta f_{i,i+1}$ and $f_{i,i+1}$ for Δf_i and f_i, respectively, the frequency resolution shown in Eq. (15) can be rewritten to determine the separation $\Delta f_{i,i+1}$ in the form

$$\Delta f_{i,i+1} \geqslant (2\alpha)\frac{f_{i,i+1}}{2\pi\sqrt{f_b} f_c}, \tag{16}$$

which can also be employed to determine the ranges of the parameter f_b and f_c in the following form:

$$\sqrt{f_b} f_c \geqslant (2\alpha) \frac{f_{i,i+1}}{2\pi \Delta f_{i,i+1}}, \tag{17}$$

where α is the parameter defining how much overlap is allowed between the adjacent Gaussian windows of the modified Morlet wavelet is allowed. Generally, when $\alpha = 1$, the windows centered at two frequencies will overlap to be inseparable. For traditional Morlet wavelet, Kijewski and Kareem [12] suggested that $\alpha = 2$ is generally sufficient to distinguish two adjacent frequency components, which however is considered in an empirical way. Note that increasing α indicates the increase of $\sqrt{f_b} f_c$, which however results in the decrease of time resolution. In this study, we loose the threshold value down to $\alpha = 1.5$ so that in some severe cases a certain compromise can be achieved between the time and frequency resolutions.

Another attention is the end-effect, which has inevitable influence on the quality of the wavelet coefficients. Based on Kijewski and Kareem's study [12], the regions of the two ends of the ith modal response to be removed is determined by

$$\Delta T_i = \beta \Delta t_i = \beta \frac{f_c}{f_i} \frac{\sqrt{f_b}}{2}, \tag{18}$$

where β is an integer value determined according to the desired accuracy level. It is seen that the lowest frequency yields the maximum end-effect. In general, when $\beta \geqslant 4$, the end-effect regions can be sufficiently eliminated. Note that if $\Delta T_i \leqslant \gamma T$ is predetermined to limit the range of the end-effect, to guarantee sufficient signal segments for analysis, with Eq. (18) as a basis, the corresponding $\sqrt{f_b} f_c$ should satisfy the following condition

$$\sqrt{f_b} f_c \leqslant \left(\frac{2\gamma}{\beta}\right) T f_i, \tag{19}$$

where γ is practically set to be less than 0.4, which reveals that at least 20% of the signal should be preserved for further analysis.

Thus, indications for the determining of the parameters f_b and f_c considering the modal separation in the frequency domain and the end-effect segments in the time domain were constructed as given in Eqs. (17) and (19).

2.3.2. Parameter selection

In the case of determining the values of $\sqrt{f_b} f_c$, it is obtained that $\sqrt{f_b} f_c \geqslant \sqrt{2}$ is easy to be satisfied and thus combining Eq. (17) with Eq. (19), the product $\sqrt{f_b} f_c$ satisfies the following inequality:

$$(2\alpha) \frac{f_{i,i+1}}{2\pi \Delta f_{i,i+1}} \leqslant \sqrt{f_b} f_c \leqslant \left(\frac{2\gamma}{\beta}\right) T f_i, \tag{20}$$

which demonstrates that $\sqrt{f_b} f_c$ should be chosen within an interval so that a compromise could be made between frequency and time resolutions. For an analytical signal, the parameters T, f_i, $f_{i,i+1}$ and $\Delta f_{i,i+1}$ are known or predetermined by Fourier transform. As stated in Section 2.3.1, when assumed $\alpha = 2$, $\beta = 4$, $\gamma = 0.4$, the closely spaced modes can be entirely separated, further,

the end-effect regions can be also fully eliminated. It is important to note that, when the sampling time T is very short or there exist very closely spaced modes, Eq. (20) appears to be unsolvable. In such cases, we have to decrease the parameters α, β although the time and frequency resolutions decrease simultaneously. Another consideration is that because $\sqrt{f_b}f_c$ is within an interval, there exist numerous pairs of f_b and f_c for selection. Practically, it is necessary to introduce some other criteria to select optimum values of f_b and f_c from the candidates. In this study, the minimum Shannon entropy criterion [16] was applied to consider the diversity of the analytical signal.

Assume that $W(a_i, t)$, $i = 1, 2, \ldots, M$ is a set of wavelet coefficients. The Shannon wavelet entropy is calculated by

$$E = -\sum_{i=1}^{M} d_i \log d_i, \tag{21}$$

where

$$d_i = \frac{|W(a_i, t)|}{\sum_{j=1}^{M} W(a_j, t)}. \tag{22}$$

This criterion measures the information of each WT. In practical application, the entropy $E(f_b, f_c)$ is calculated for a range of values of f_b and f_c which should first meet the requirements of Eq. (20). The optimum value is the pair leading to the minimum value of the wavelet entropy E of the wavelet coefficients matrix $W(a, t)$.

3. Bootstrap-based uncertainty estimation

In practical applications of modal identification, the WT method as well as the traditional schemes most often supplies a single estimate of the modal parameter for each time history, and the repeated measurements for the real structure are also restricted. Hence, there is no adequate information for appropriate statistical description to consider and evaluate the impacts of uncertainties inherent on identification accuracies. Practically, these uncertainties intrinsic derived from the noise level, environmental variability, and measurement errors, are worth investigating as this may lead to a deeper understanding of the structural dynamics properties.

Due to these limitations, a simple but effective bootstrap scheme, capable of providing effective statistical inferences without the restrictions of the usual normal-theory assumptions and large enough samples, is proposed in conjunction with the WT to consider the influences of uncertainty on modal parameters.

3.1. Outline of the bootstrap theory

The bootstrap theory pioneered by Efron [15] was originally introduced to evaluate the statistical accuracy by calculating the confidence intervals of the random variables with unknown probability distribution and limited data or samples. The typical bootstrap method can be described as follows.

Suppose we observe a random independent sample $X=(x_1,x_2,\ldots,x_n)$ drawn from an unknown identical distribution F and a statistic inference of interest $\hat{\theta}=s(X)$. By randomly sampling with replacement from the original data, a bootstrap sample $X^*=\left(x_1^*,x_2^*,\ldots,x_n^*\right)$ and the corresponding estimator $\hat{\theta}^*=s(X^*)$ can be obtained. After replicating B times the bootstrap operation, B numbers of bootstrap ensemble $\left(\hat{\theta}_1^*,\hat{\theta}_2^*,\ldots,\hat{\theta}_B^*\right)$ are generated. Finally, from the histogram of the bootstrap ensemble, the probability density function can be determined and the standard deviation $\hat{s}_\theta^*$ of the values $\hat{\theta}_1^*,\hat{\theta}_2^*,\ldots,\hat{\theta}_B^*$ is the estimate of the standard error of $s(x)$, i.e.

$$\hat{s}_\theta^*=\left[\frac{1}{B-1}\sum_{b=1}^{B}\left(\hat{\theta}_b^*-\bar{\theta}^*\right)^2\right]^{1/2}, \tag{23}$$

where

$$\bar{\theta}^*=\frac{1}{B}\sum_{b=1}^{B}\hat{\theta}_b^*. \tag{24}$$

The bootstrap percentile method is used to define the confidence interval. Let $\hat{\theta}_B^{*(p)}$ be the $(100\cdot p)$th empirical percentile of the $\hat{\theta}_b^*$ values, i.e. the $(B\cdot p)$th value in the order list of the B replications of $\hat{\theta}^*$. Likewise let $\hat{\theta}_B^{*(1-p)}$ be the $100\cdot(1-p)$th empirical percentile. The approximate percentile confidence interval at level $1-2p$ is then determined as

$$\left[\hat{\theta}_{\%,\mathrm{low}},\hat{\theta}_{\%,\mathrm{up}}\right]\approx\left[\hat{\theta}_B^{*(p)},\hat{\theta}_B^{*(1-p)}\right]. \tag{25}$$

If the number of bootstrap B is large enough, the bootstrap histogram will become normal shaped, and thus an accurate confidence interval can be obtained.

3.2. Bootstrap schemes in WT-based parameter identification

When dealing with the measurement signal, different statistical analyses of the time series and dynamic models through the use of bootstrap have been derived in order to obtain accurate results of the modal parameters. Bittanti and Lovera [18] proposed the application of the bootstrapping residues methods to the problem of evaluating model uncertainty in the framework of the input/output subspace identification models. Kijewski and Kareem [19] presented a basic bootstrap approach to assess the quality of the system identification by providing surrogate estimates of damping and natural frequency to generate useful statistics and confidence intervals.

For the present purpose, in the case of free decay signal, assume S experimental tests are implemented and B bootstrap samples are generated. Based on the bootstrap procedure described in Section 3.1, we can acquire the bootstrap distribution and confidence interval of the modal parameter. For output-only system, in general, the well-known RDT is preprocessed to extract the free decay responses from the ambient vibration data for further identification. In this paper, based on the basic form of the bootstrap, a procedure for the estimation of standard error and confidence interval of the modal parameter from output-only data is presented in the framework of the WT-only based modal identification scheme. As shown in

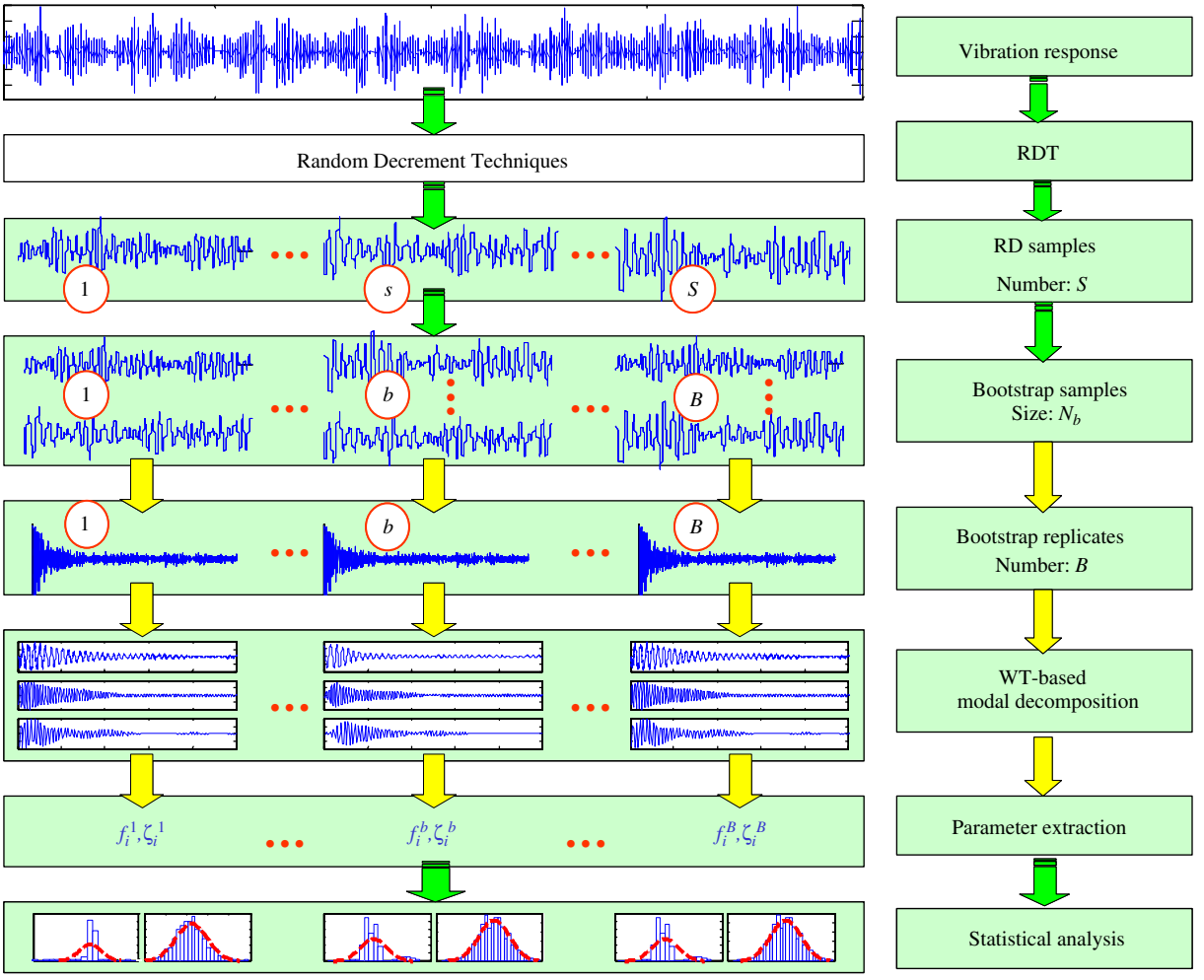

Fig. 1. Bootstrap scheme for WT-based modal identification.

Fig. 1, S random decrement (RD) segments satisfying the triggering condition are extracted from the measured response and form a sample population. Each bootstrap sample has N_b RD segments, formed by sampling with replacement N_b times from S RD sample population. Then, each bootstrap sample is averaged to form a smoothed RD signal for WT-based parameter identification. This procedure is repeated B times to generate B replicates of the modal parameters. Finally, the statistical analysis based on Eqs. (23)–(25) is implemented to estimate the standard error and confidence interval of the modal parameter. It is important to note that the bootstrap method deals correctly only with independent and identically distributed random data set. Generally, each RD segment satisfying a triggering condition is randomly drawn from the measured vibration response, thus it is readily extensible to consider it as an independent random sample.

4. Applications

4.1. Numerical simulation

The WT-based modal identification in conjunction with the bootstrap method is first tested on a simulated 3dof damped system with two closely spaced modes. The parameters based on Eq. (6) are configured as follows: $f_1 = 1.0\,\text{Hz}$; $f_2 = 1.06\,\text{Hz}$; $f_3 = 2.0\,\text{Hz}$; $\zeta_i = 0.01$; $A_i = 1.0$; $\theta_i = 0$ $(i = 1, 2, 3)$; sampling frequency $f_s = 20\,\text{Hz}$ and sampling time $T = 60\,\text{s}$. Obviously, for these two closely spaced modes, $f_{1,2} = 1.03\,\text{Hz}$, $\Delta f_{1,2} = 0.06\,\text{Hz}$.

To ensure sufficient time-frequency resolution, $\alpha = 1.5$, $\beta = 4$, and $\gamma = 0.4$ are assumed for further analysis. By substituting all the parameter values into Eq. (20), we obtain $8.2 \leqslant \sqrt{f_b} f_c \leqslant 12.0$. Fig. 2(a) uses two vertical axes, left vertical axis representing variation of minimum wavelet entropy E via Eq. (21) and right one representing variation of the product $\sqrt{f_b} f_c$, to get an insight in the relationships among the parameters. It is seen that all the values of $\sqrt{f_b} f_c$ are within the interval [8.2 12.0] when $f_c > 1.5$, particularly when $f_c = 2.5$, the wavelet entropy E obtains its minimum value. Fig. 2(b) presents the variations of wavelet entropy with respect to f_b when $f_c = 2.5$. It is observed that there exists an optimum value of $f_b = 17$ leading to minimum wavelet entropy. The corresponding results of modal separation, phase angle $\varphi(t)$ and logarithm of amplitude $\ln[B(t)]$ are displayed in Fig. 3. It is seen that these two closely spaced modes are fully separated, and the end-effect regions can be clearly indicated and eliminated when β is set to be 4. Moreover, it is obviously found that the end-effect for low-frequency mode has more serious impact than that for the high-frequency mode.

Table 1 gives a comparison of the damping ratio errors with different parameter configurations. Note that the noise contamination is generally inevitable. The simulated signal corrupted by noise level R_i is defined as $x_i(t) = x(t)(1 + rR_i)$, where r is a normally distributed random variable with zero mean and unit variance ("standard noise"). From Table 1, it is observed that when $\alpha = 1$, the frequency resolution is lower, and these two closely spaced modes cannot be identified. Increasing α results in increase of the frequency resolution and decrease of the time resolution. When $\alpha = 3$ and $\beta = 4$, the length of the end-effect region (32.8 s for the first mode and 31.0 s for the second mode) is even beyond the half-length of the analytical signal (30 s), which makes it fail to identify

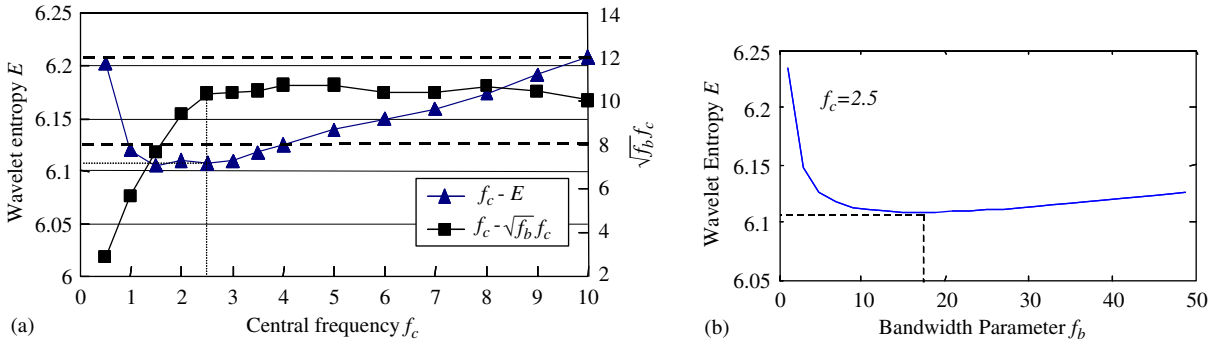

Fig. 2. (a) Relationship between the wavelet entropy E and two parameters f_b and f_c, dotted horizontal line demarks the interval of $\sqrt{f_b} f_c$ and (b) variations of the wavelet entropy with respect to f_b in the case of $f_c = 2.5$.

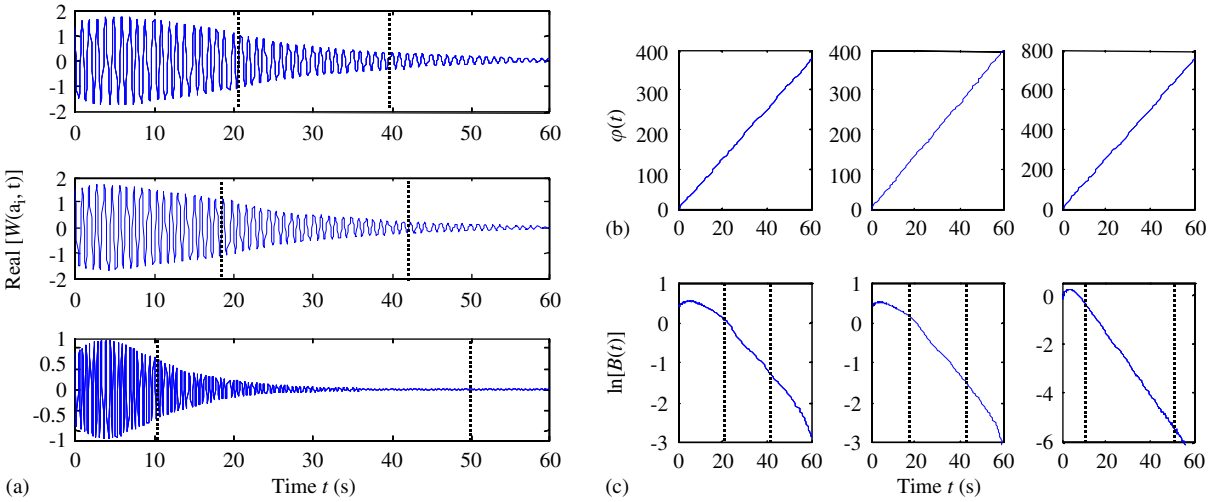

Fig. 3. (a) The WT-based modal separation for the first mode (top), second mode (middle), and third mode (bottom); (b) the phase angle $\varphi(t)$ and (c) the semi-logarithm of amplitude $\ln[A(t)]$ for the first mode (left), second mode (middle) and third mode (right). Dotted vertical lines demarcate the end-effect regions when $\beta = 4$.

Table 1
Variation of damping ratio error (%) with different parameter configurations

Mode			Noise level R				Noise level R				Noise level R		
	ΔT_i (s)	Δf_i (Hz)	0%	40%	ΔT_i (s)	Δf_i (Hz)	0%	20%	40%	ΔT_i (s)	Δf_i (Hz)	0%	20%	40%
	$f_b = 4.78, f_c = 2.5$				$f_b = 17, f_c = 2.5$					$f_b = 43.0, f_c = 2.5$				
	$\alpha = 1, \beta = 0$				$\alpha = 1.89, \beta = 0$					$\alpha = 3, \beta = 0$				
1	0.00	0.029	—	—	0.00	0.015	9.47	9.46	8.76	0.00	0.010	15.9	17.7	17.1
2	0.00	0.031	—	—	0.00	0.016	8.66	8.83	8.76	0.00	0.010	8.61	8.53	8.48
3	0.00	0.058	2.83	13.7	0.00	0.031	4.42	6.83	19.1	0.00	0.019	9.36	8.44	8.73
	$\alpha = 1, \beta = 4$				$\alpha = 1.89, \beta = 4$					$\alpha = 3, \beta = 4$				
1	10.9	0.029	—	—	20.6	0.015	1.42	2.28	7.29	32.8	0.010	—	—	—
2	10.3	0.031	—	—	19.4	0.016	0.64	1.92	3.18	31.0	0.010	—	—	—
3	9.48	0.058	0.02	23.5	10.3	0.031	0.02	1.72	9.62	16.4	0.019	0.08	2.49	7.51

the system. Further, when the impacts of end-effect are not considered ($\beta = 0$), there are discrepancies in the identified damping ratios no matter whether the noise level is higher or lower. Note that in the cases of the optimum values of $f_b = 17, f_c = 2.5$ (the corresponding α is equal to 1.89) for modal separation and $\beta = 4$ for fully considering the end-effect, when the noise level is lower, the excellent identification results can be obtained. However, the higher noise level such as 40% yields poor identification results. For instance, the damping ratio error of the third mode increase to 9.62%.

Table 2
Statistical analysis for damping ratio estimation using bootstrap scheme

	$\alpha = 1.89$ $\beta = 0$ $S = 50$ $B = 1000$					$\alpha = 1.89$ $\beta = 4$ $S = 50$ $B = 1000$				
	$R = 0$	$R = 40\%$				$R = 0$	$R = 40\%$			
Mode (i)	ζ_i (%)	$\sigma(\zeta_i)$[a] (%)	ζ_i^{boot} [b] (%)	CoV_i[c] (%)	95% Boot[d] (%)	ζ_i (%)	$\sigma(\zeta_i)$ (%)	ζ_i^{boot} (%)	CoV_i (%)	95% Boot (%)
1	0.905	1.81E-3	0.905	0.201	(0.902, 0.908)	0.986	5.20E-3	0.977	0.532	(0.969, 0.986)
2	0.913	2.01E-3	0.913	0.222	(0.909, 0.916)	0.994	5.58E-3	0.989	0.564	(0.980, 0.998)
3	0.956	1.11E-2	0.939	1.181	(0.922, 0.957)	1.000	1.27E-2	0.976	1.298	(0.956, 0.997)

[a]Standard deviation of damping ratio.
[b]Bootstrap mean damping ratio.
[c]Coefficient of deviation, and $\text{CoV}_i = \sigma(\zeta_i)/\zeta_i^{\text{boot}}$.
[d]95% Confidence interval of damping ratio.

Consequently, it is seen that in the framework of WT-only based method the noise level has inevitable influences on the identification accuracies no matter whether the modal separation and end-effect are considered or not.

On the other hand, because of the randomness of the noise pollution, even if all the time histories are contaminated by the same noise level, each of the estimated modal parameters has a little discrepancy and is subject to a certain distribution. The bootstrap method is presented for statistical inference.

Let us consider a sample population containing $S = 50$ signal elements simulated by each introducing 40% noise level to the above-proposed simulated signal. Then $B = 1000$ bootstrap samples are generated from the given sample population. The optimum parameters for the WT-based identification are configured as $f_b = 17$, $f_c = 2.5$, $\alpha = 1.89$. The statistical inference results for damping ratios are illustrated in Table 2. It is observed that, when $\beta = 0$, i.e. not removing the end-effect segments, the bootstrap mean damping ratios $\zeta_1^{\text{boot}} = 0.905\%$ for the first mode and $\zeta_2^{\text{boot}} = 0.913\%$ for the second mode are, respectively, equal to ζ_1 and ζ_2 where noises are not introduced. Moreover, note that in the case of $\beta = 4$, i.e. the end-effect regions are entirely eliminated, the bootstrap mean damping ratios are in agreement with those without noise contamination. Consequently, compared with Table 1, the bootstrap method has the capability to make a statistical inference from the limited samples, which obviously implies that it supplies more valuable identification information than the WT-only based method. Another advantage is that the confidence interval of modal parameter can be used to indicate the impacts of uncertainty.

It is important to note that, although the bootstrap can draw valid statistical inferences, its performance is still dependent on the quality of the RD data and the effectiveness of the WT-only based identification method. For instance, when the end-effect is not considered, though the bootstrap method can indicate the uncertainty, for the first mode, there still exists greater relative error up to about 9.5% between the bootstrap mean value and the theoretical value. However, in the case that the end-effect is entirely removed when $\beta = 4$, there exists only about 2.3% relative error even when the noise level increases to 40%.

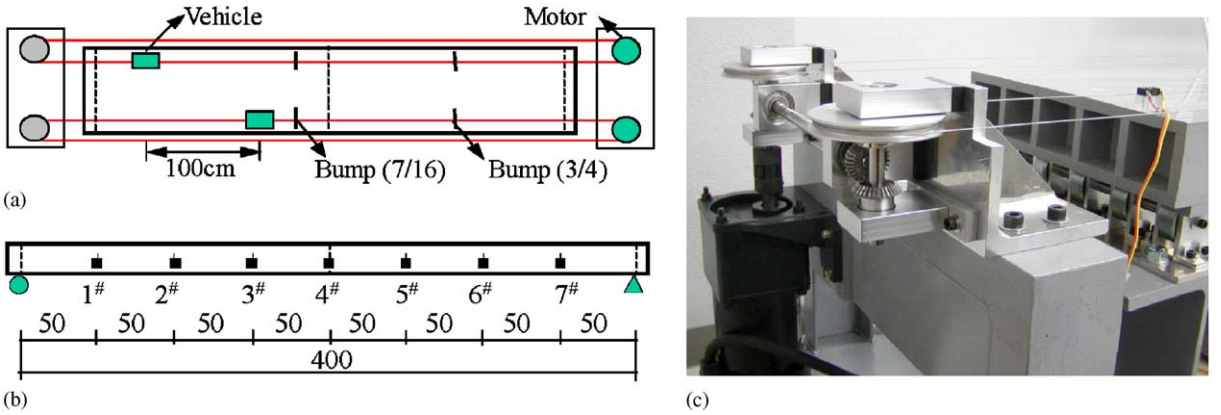

Fig. 4. (a) Experimental setup; (b) sensor placement (unit: cm) and (c) rope gearing system.

4.2. Experimental verification

4.2.1. Experimental setup

The bridge model made up of polycarbonate plastic is 400 cm long, 31 cm wide, and 7 cm high. As represented in Fig. 4, the cross-section of the beam is a box girder with five rooms. Two bumps and two vehicles each with a 10 N weight are configured to simulate the traffic loading as an ambient random excitation to the bridge model. A rope gearing system is set to pull these two vehicles with an interval of 100 cm along the bridge deck back and forth with different running speeds. To measure the vibration responses, seven piezoresistive accelerometers (flat frequency response: 0–50 Hz) are installed evenly at the side surface of the $\frac{1}{8}$ points of the beam. The DC-104R is used to acquire and record the vibration response data. The sampling frequency of the digital recorder is fixed at 100 Hz, the sampling time is 280 s.

4.2.2. Results

An example of acceleration time history at the location of $2^{\sharp}$ (see Fig. 4) is plotted in Fig. 5(a). The RDT is applied to the time history to obtain the RD signature. In this case, the length of RD signature is determined as 1024 points (10.24 s), a triggering level of $[1.2\sigma + \infty]$ (σ: standard deviation of the time history) is selected, and the number of triggering points is set to be $S = 2776$. The RD signature is shown in Fig. 5(b). It is seen that the noise level appears to be severe. From the impact test, it is observed that there exist three well-separated modes around 3.8, 15.2 and 32.5 Hz. Hence, it is easy to consider the time–frequency resolution properties of the RD signature. Fig. 6(a) presents the relationship between the wavelet entropy E and two parameters f_b and f_c. By Eq. (20), it is calculated that all the values of $\sqrt{f_b} f_c$ are within the interval [0.53 7.94] when $f_c \geqslant 0.5$, particularly when $f_c = 1.0$, the wavelet entropy E obtains its minimum value. Fig. 6(b) presents the variations of wavelet entropy with respect to f_b. It is clear that an optimum value of $f_b = 17$ leads to minimum wavelet entropy. The phase angle $\varphi(t)$ and semi-logarithm of amplitude $\ln[B(t)]$ are plotted in Figs. 5(c) and (d). It is important to note that, in the case of impact test, for the second and the third modes, only the first 5 and 2 s of the separated modal

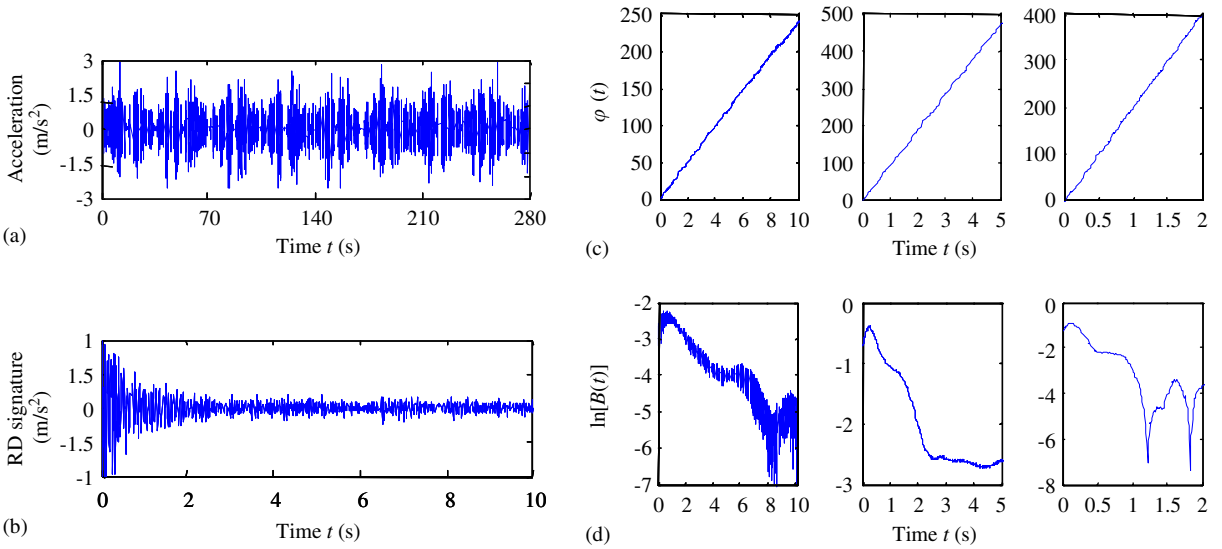

Fig. 5. (a) Time history at the location of $2^{\sharp}$ (see Fig. 4.); (b) RD signature; (c) phase angle and (d) semi-logarithm of amplitude for the first, the second and the third modes (from left to right).

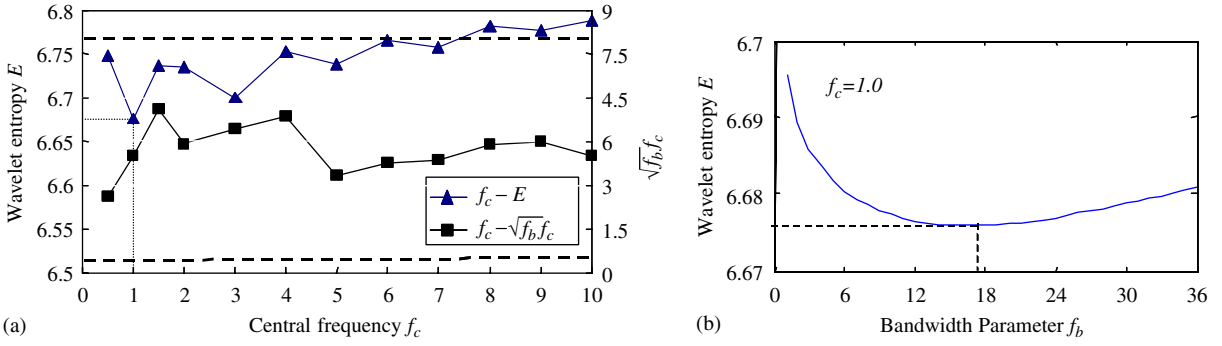

Fig. 6. (a) Relationship between the wavelet entropy E and two parameters f_b and f_c and (b) variations of the wavelet entropy with respect to f_b when $f_c = 1.0$. Dotted horizontal line demarks the interval of $\sqrt{f_b} f_c$.

signal with relatively linear and stable characteristics are, respectively, extracted as the analysis length. For comparison, the same length is set for the ambient vibration test.

From Figs. 5(c) and (d), it is observed that the semi-logarithms of amplitudes are capable of indicating the end-effect regions. Notice that some segments of them are far away from linearity due to the poor quality of the RD signature. One of the reasons is that, strictly speaking, the traffic loadings simulated by two vehicles with different running speeds and impacts derived from two bumps do not properly satisfy the assumption of white noise, and further, the effects of noise contamination are also very high. Hence in the process of RDT, the random part of the random response cannot be averaged to a zero vector, which results in the deterministic part to be preserved as a free-decay response contaminated by inevitable noise.

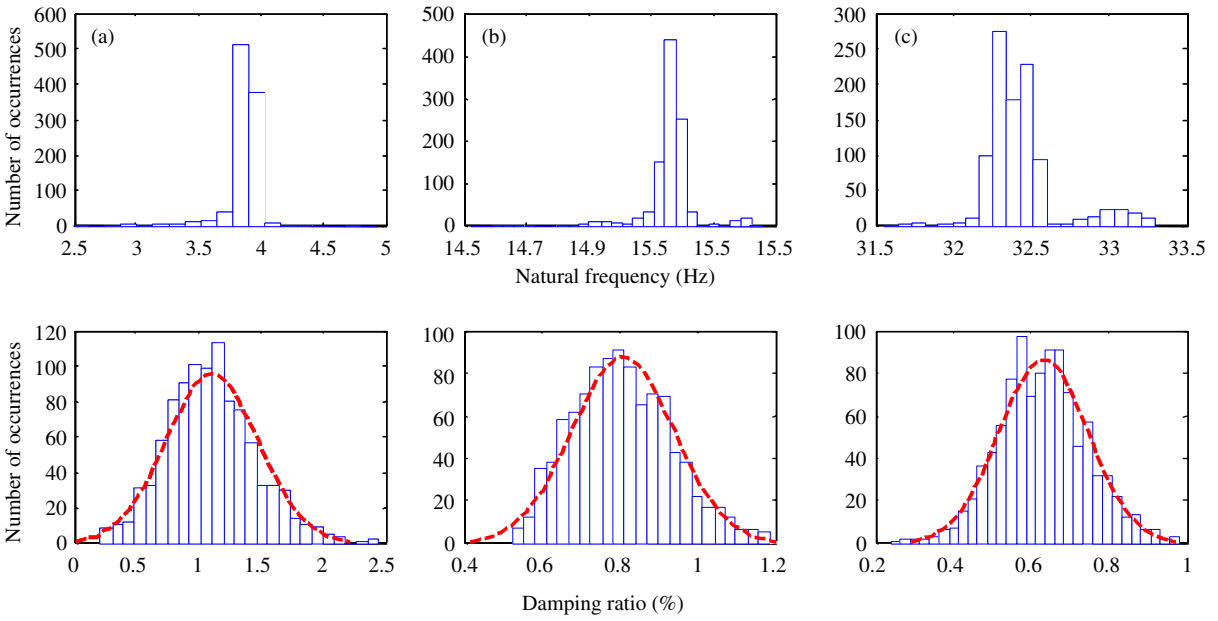

Fig. 7. Histogram of bootstrap estimation results on the natural frequency (top) and damping ratio (bottom) for the (a) first mode; (b) second mode and (c) third mode.

Table 3
Overview of the parameter identification results for bridge model test

	Modal parameters		End-effect		Confidence interval (95% boot)	
Mode	Frequency (Hz)	Damping ratio (%)	ΔT_L (s)	ΔT_R (s)	Frequency (Hz)	Damping ratio (%)
Impact test (*sampling frequency*: 100 Hz; *sampling time*: 10.24 s)						
1	3.878	1.122	2.98	2.98	— —	— —
2	15.625	0.751	0.76	5.24	— —	— —
3	34.485	0.784	0.36	8.24	— —	— —
Ambient vibration test (*Sampling time*: 280 s; *RD signature*: 10.24 s)						
1	3.846	1.090	2.10	2.10	— —	— —
2	15.134	0.479	0.51	5.24	— —	— —
3	32.525	0.758	0.24	8.24	— —	— —
Statistics of bootstrap replications of modal parameters based on ambient vibration test ($N_b = 2500$, $B = 1000$)						
1	3.842[a]	1.093[b]	2.10	2.10	[3.540, 3.932]	[0.552, 1.742]
2	15.161[a]	0.807[b]	0.51	5.24	[15.066,15.254]	[0.612, 1.041]
3	32.434[a]	0.632[b]	0.24	8.24	[32.195,33.047]	[0.463, 0.823]

[a]Bootstrap mean natural frequency.
[b]Bootstrap mean damping ratio.

The bootstrap scheme shown in Fig. 1 is employed to consider uncertainty. Each bootstrap sample containing $N_b = 2500$ elements is randomly sampled from $S = 2776$ RD samples, and $B = 1000$ bootstrap replicate samples are generated for further statistical analysis. The histograms

of the bootstrap estimation results for modal parameters are displayed in Fig. 7. Note that the distributions of the estimated natural frequencies are concentrated, whereas for the damping ratios, the distributions are more scattered and generally in accordance with the normal distribution. Table 3 gives the comparisons of the identification results derived from the impact test and ambient vibration test considering the end-effect. It is observed that the WT-only based method is effective for the estimation of natural frequency, however, for the damping ratio estimation, due to the poor quality of the RD signature, the estimated damping ratio 0.479% for the second mode is even beyond 95% confidence interval [0.612%, 1.041%] offered by bootstrap scheme. Furthermore, the bootstrap mean natural frequencies and damping ratios are, respectively, close to those obtained by impact test with relative higher identification accuracies. In addition, it is important to note that, due to the influences of vehicle weights, the natural frequencies estimated by the ambient vibration test are smaller than those based on the impact test.

5. Conclusions

In this contribution, an integrated identification method based on WT and bootstrap theory has been proposed for considering uncertainty effect on modal parameter.

It has been revealed that, by carefully considering the influences of modal separation, end-effect and parameters of wavelet function on identification accuracies, the WT-only based method is very suitable for identifying system with closely spaced modes. Moreover, it has been shown that the proposed bootstrap method is capable of making up the inadequacy of the WT-only based method when dealing with uncertainty.

The integrated procedures have been applied to a numerical simulation and a bridge model test giving satisfactory results of modal parameter estimation. Particularly for the output-only system with poor quality of RD signature, the bootstrap scheme offers statistical information such as bootstrap mean value and confidence interval of modal parameters, and the accuracy of the integrated method in considering uncertainty effect is remarkable.

Further work will place emphases on the parameter selection and model selection for the bootstrap scheme and on the test for the real bridges. Another interest is that in the implementation of the bootstrap to the RD signature, in a strict sense, the RD segments do not entirely satisfy the condition that each of them has to be an independent and identically distributed sample. Thus the methods for overcoming this limitation will be the topic of future investigation.

Acknowledgments

The authors gratefully acknowledge for the support of this research work by the Grant-in-Aid for Scientific Research (S) on "Strategic Life-Cycle Management for Civil Infrastructure Systems with the Latest Information Technologies" of JSPS.

References

[1] S.W. Doebling, C.R. Farrar, M.B. Prime, D.W. Shevitz, Damage identification and health monitoring of structural and mechanical systems from changes in their vibration characteristics. A literature review, Report LA-13070-MS, Uc-900, Los Alamos National Laboratory, New Mexico, 1996.

[2] S.W. Doebling, C.R. Farrar, The state of the art in structural identification of constructed facilities, A Report by the ASCE Committee on Structural Identification of the Constructed Facilities, 1999.

[3] K.F. Alvin, A.N. Robertson, G.W. Reich, K.C. Park, Structural system identification: from reality to models, *Computers & Structures* 81 (2003) 1149–1176.

[4] S. Qian, *Introduction to Time–frequency and Wavelet Transforms*, Prentice-Hall PTR, Englewood Cliffs, NJ, 2002.

[5] S.A. Neild, P.D. McFadden, M.S. Williams, A review of time–frequency methods for structural vibration analysis, *Engineering Structures* 25 (2003) 713–728.

[6] J.B. Bodeux, J.C. Golinval, Application of ARMAV models to the identification and damage detection of mechanical and civil engineering structures, *Smart Materials and Structures* 10 (2001) 479–489.

[7] J.M. Ndambi, B. Peeters, J.De. Visscher, M.A. Wahab, J. Vantomme, G.De. Roeck, W.P. Wilde, Comparison of techniques for modal analysis of concrete structures, *Engineering Structures* 22 (2000) 1159–1166.

[8] G.H. James, T.G. Garne, J.P. Lauffer, The Natural excitation technique (NExT) for modal parameter extraction from operating wind turbines, Report SAND92-1666, UC-261, Sandia national Laboratories, Albuquerque, New Mexico, 1993.

[9] Q. Qin, H.B. Li, L.Z. Qian, Modal identification of Tsing Ma bridge by using improved eigensystem realization algorithm, *Journal of Sound and Vibration* 247 (2001) 325–341.

[10] W.J. Staszewski, Identification of damping in mode system using time-scale decomposition, *Journal of Sound and Vibration* 203 (1997) 283–305.

[11] J. Lardies, S. Gouttebroze, Identification of modal parameters using the wavelet transform, *International Journal of Mechanical Science* 44 (2002) 2263–2283.

[12] T. Kijewski, A. Kareem, Wavelet transforms for system identification in civil engineering, *Computer-aided Civil and Infrastructure Engineering* 18 (2003) 339–355.

[13] B.F. Yan, A. Miyamoto, S. Goto, A comparison of wavelet transform and Hilbert–Huang transform for modal parameter extraction of structure, *Journal of Applied Mechanics JSCE* 7 (2004) 1167–1178.

[14] J.N. Yang, Y. Lei, S.W. Pan, N. Huang, System identification of linear structures based on Hilbert–Huang spectral analysis, Part 1: normal modes, *Earthquake Engineering Structure* 32 (2003) 1533–1554.

[15] B. Efron, R. Tibushirani, *An Introduction to the Bootstrap*, Chapman & Hall, London, 1993.

[16] J. Lin, L. Qu, Feature extraction based on Morlet wavelet and its application for mechanical fault diagnosis, *Journal of Sound and Vibration* 234 (2000) 135–148.

[17] Y.T. Sheen, C.K. Huang, Constructing a wavelet-based envelope function for vibration signal analysis, *Mechanical System and Signal Processing* 18 (2004) 119–126.

[18] S. Bittanti, M. Lovera, Bootstrap-based estimates of uncertainty in subspace identification methods, *Automatica* 36 (2000) 1605–1615.

[19] T. Kijewski, A. Kareem, On the reliability of a class of system identification techniques: insights from bootstrap theory, *Structural Safety* 24 (2002) 261–280.